INORGANIC CHEMISTRY FRONTIERS

RESEARCH ARTICLE

View Article Online
View Journal | View Issue



Cite this: *Inorg. Chem. Front.*, 2023, **10**, 7343

# From $CdPb_8(SeO_3)_4Br_{10}$ to $Pb_3(TeO_3)Br_4$: the first tellurite bromide exhibiting an SHG response and mid-IR transparency†

Peng-Fei Li, [a,b] Chun-Li Hu,[a] Bing-Xuan Li,[a] Jiang-Gao Mao [a,b] and Fang Kong *[a,b]

Received 22nd September 2023,
Accepted 25th October 2023

DOI: 10.1039/d3qi01937c

rsc.li/frontiers-inorganic

Herein, we report two new selenite/tellurite bromide compounds, namely, $CdPb_8(SeO_3)_4Br_{10}$ and $Pb_3(TeO_3)Br_4$. The former crystallized in a centrosymmetric space group, while the latter is a non-centrosymmetric compound. Specifically, $CdPb_8(SeO_3)_4Br_{10}$ demonstrates high thermal stability (425 °C) and a wide optical transparency window (0.33–6.5 μm), while $Pb_3(TeO_3)Br_4$ exhibits an second harmonic generation response approximately equivalent to that of KDP, appropriate birefringence (0.095@532 nm and 0.066@1064 nm), wide optical transparency window (0.33–6.5 μm) and high thermal stability (522 °C). These results indicated that lead tellurite bromides could be promising nonlinear optical material systems in the mid-IR wavelength.



## Introduction

Nonlinear optical (NLO) crystals are widely used in various fields such as frequency conversion, optical modulation, optical switching and limiting, optical sensing, remote sensing, environmental monitoring, and free-space communications.[1–6] Second-order nonlinear optical materials require compounds to crystallize in non-centrosymmetric (NCS) space groups.[7–10] According to the ICSD database, the probability of obtaining a non-centrosymmetric structure is less than 20%.[11–13] So, the rational design of inorganic compounds with non-centrosymmetric symmetry remains a challenging but beneficial task for researchers in chemical and materials science.

Selenite and tellurite compounds are important systems for exploring NLO materials.[14] The coordination environment of $Se^{4+}$ and $Te^{4+}$ is inherently polar due to the presence of stereochemically active lone pairs (SALP) of electrons, with oxygen ligands being located on one side of the cations.[15,16] Researchers have made significant efforts to enhance the probability of obtaining NCS selenite and tellurite crystals. In this endeavor, one effective strategy employed is to combine different nonlinear active groups within a single structure.[17] Known nonlinear active units include, but are not limited to, $d^0$ transition metal octahedra ($TiO_6$, $MoO_6$, $WO_6$, $VO_6$, $NbO_6$, *etc.*),[11,18] and their derivatives ($GaO_6$, $GaO_3F_3$, *etc.*),[19–21] $d^{10}$ transition metals with large polar displacement ($Zn^{2+}$, $Cd^{2+}$, $Hg^{2+}$),[22,23] and SALP cations ($Pb^{2+}$, $Bi^{3+}$, $Sn^{2+}$, $Sb^{3+}$, *etc.*).[24,25] Some high-performance NLO materials have been explored, such as $Pb_2(SeO_3)(NO_3)_2$ (2 × KDP),[26] $NaNbO(SeO_3)_2$ (7.8 × KDP),[18] $LiNbTeO_5$ (17 × KDP),[27] $Cd_2Nb_2Te_4O_{15}$ (31 × KDP),[28] β-$BaTeW_2O_9$ (1.5 × KTP)[29] and $TlSb_3Te_2O_{12}$ (37.2 × KDP).[30] Furthermore, replacing the oxygen atoms in the coordination with VIIA anions is another effective approach for obtaining NCS compounds.[31,32] For example, the first UV NLO selenite, $Y_3F(SeO_3)_4$ (5.5 × KDP), was created through a fluorination control strategy.[33] $Ba(MoO_2F)_2(TeO_3)_2$, containing partially fluorinated $MoO_6$ octahedra, can demonstrate a large second harmonic generation (SHG) intensity (7.8 × KDP).[34] Additionally, some halogenated selenite/tellurite compounds, such as $Pb_2GaF_2(SeO_3)_2Cl$ (4.5 × KDP),[35] $Pb_2Bi(SeO_3)_2Cl_3$ (13.5 × KDP),[36] $Cs(TiOF)_3(SeO_3)_2$ (5 × KDP),[37] $RbGa_3F_6(SeO_3)_2$ (5.6 × KDP),[38] $BaF_2TeF_2(OH)_2$ (3 × KDP)[39] and $RbTeMo_2O_8F$ (27 × KDP),[40] also exhibit excellent SHG effects. Based on literature research, it can be observed that most of the research on halogenated selenite/tellurite NLO materials focuses on $F^-$ and $Cl^-$, while there is relatively less research on $Br^-$ and $I^-$. Only the following selenites, $Pb_2NbO_2(SeO_3)_2Br$ (1.4 × KDP),[41] $Pb_2GaF_2(SeO_3)_2Br$ (4.5 × KDP),[41] $Pb_2Cd(SeO_3)_2Br_2$ (1.4 × KDP),[17] and $Pb_3(SeO_3)Br_4$ (1 × KDP),[42] have been reported to exhibit SHG effects.

Generally, $Br^-$ and $I^-$ anions have higher polarizability and lower electronegativity compared to $F^-$ and $Cl^-$ anions.[43] This

[a]*State Key Laboratory of Structural Chemistry, Fujian Institute of Research on the Structure of Matter, Chinese Academy of Sciences, Fuzhou 350002, P. R. China. E-mail: kongfang@fjirsm.ac.cn*
[b]*University of Chinese Academy of Sciences, Beijing 100049, P. R. China*

†Electronic supplementary information (ESI) available: Detailed synthesis, PXRD patterns, crystal data, TG curves, UV-vis-NIR diffuse-reflectance spectra, IR spectra, and computational method. CCDC 2278543 for $CdPb_8(SeO_3)_4Br_{10}$ and 2278544 for $Pb_3(TeO_3)Br_4$]. For ESI and crystallographic data in CIF or other electronic format see DOI: https://doi.org/10.1039/d3qi01937c

leads to more favorable effects of $Br^-$ and $I^-$ anions on the SHG efficency.[42,44,45] Additionally, heavier elements such as $Br^-$ and $I^-$ are more helpful for transparency in the mid-infrared (MIR) range.[46] Based on this, we conducted research on halide selenite/tellurite compounds. To achieve high transparency in the MIR spectrum and increase the probability of obtaining NCS compounds, we have chosen the heavy element Pb(II) and $d^{10}$ TM Cd(II) as counter cations. After numerous attempts, we have synthesized a new compound of $CdPb_8(SeO_3)_4Br_{10}$ through mild hydrothermal reactions. Unfortunately, $CdPb_8(SeO_3)_4Br_{10}$ crystallized in a centrosymmetric (CS) space group. Through structural analysis, we found that the cadmium is surrounded by four $SeO_3$ groups and the polarity of the SALP $Se^{4+}$ was almost cancelled out in the $[Cd(SeO_3)_4]^{6-}$ unit. In order to achieve the structural transformation from CS to NCS, such an unfavourable arrangement should be changed.[47] We attempted to remove the $CdO_6$ groups from the structure, and introduce larger $Te^{4+}$ cations to support the framework. Ultimately, we successfully obtained the compound $Pb_3(TeO_3)Br_4$, which crystallized in an NCS space group. It is worth noting that $Pb_3(TeO_3)Br_4$ is the first reported NLO material with SHG activity and exhibits good transparency in the MIR region. Here, we provide a detailed description of their synthesis, crystal structures, thermal stability, and optical properties.

## Results and discussion

$CdPb_8(SeO_3)_4Br_{10}$ and $Pb_3(TeO_3)Br_4$ were synthesized using a mild hydrothermal synthesis method. Details of the synthesis can be found in the ESI (ESI Experimental section†). Additionally, their powder X-ray diffraction (PXRD) patterns were recorded and found to perfectly match those of simulated data, indicating that the obtained samples are produced in pure phases (Fig. S1†). The crystallographic data of $CdPb_8(SeO_3)_4Br_{10}$ and $Pb_3(TeO_3)Br_4$ are listed in ESI Table S1.†

$CdPb_8(SeO_3)_4Br_{10}$ crystallizes in the *C*2/*c* (*No. 15*) space group with a CS structure. Its asymmetric unit contains one Cd, four Pb, two Se, five Br, and six O atoms, totalling eighteen atoms. Only Cd(1) occupies a special position with an occupancy of 0.5. In the structure, Cd(1) is coordinated with six O atoms forming a $CdO_6$ octahedron with Cd–O bond lengths in the range of 2.263–2.617 Å. The Se atoms are connected with three O atoms forming $SeO_3$ trigonal pyramids with Se–O bond lengths ranging from 1.692 to 1.736 Å. The Pb atoms are connected with O and Br atoms, with Pb–Br and Pb–O bond lengths in the range of 3.022–3.193 Å and 2.435–2.734 Å, respectively. Bond valence calculations revealed that Cd(1), Pb(1)–Pb(4), and Se(1)–Se(2) exhibit bond valences of 1.744, 1.492–2.039, and 3.922–4.036, respectively. The deviation of Pb(1), Pb(2) and Pb(4) from their ideal oxidation states can be attributed to their fewer primary coordination bonds and longer secondary coordination bonds that are often overlooked in calculations. This phenomenon is a common occurrence in lead-containing compounds, as evidenced by some previously reported compounds.[48] If longer Pb···Br distances were considered, the BVS of Pb(1)–Pb(4) can be raised to 1.885–2.039.

$CdPb_8(SeO_3)_4Br_{10}$ features a novel three-dimensional (3D) network structure composed of a lead oxybromide framework decorated with $CdO_6$ octahedra and $SeO_3$ trigonal pyramids (Fig. 1). One $CdO_6$ octahedron is connected with four $SeO_3$ groups *via* edge- and corner-sharing to form a $[Cd(SeO_3)_4]^{6-}$ unit (Fig. S2a†). Two $Pb(1)O_5Br_1$ and two $Pb(2)O_5Br_1$ units are connected *via* oxygen atoms to form $Pb_4O_{12}Br_4$ tetramers (Fig. S2b†). The $Pb(3)O_2Br_6$ and $Pb(4)O_2Br_3$ units share bromine atoms to

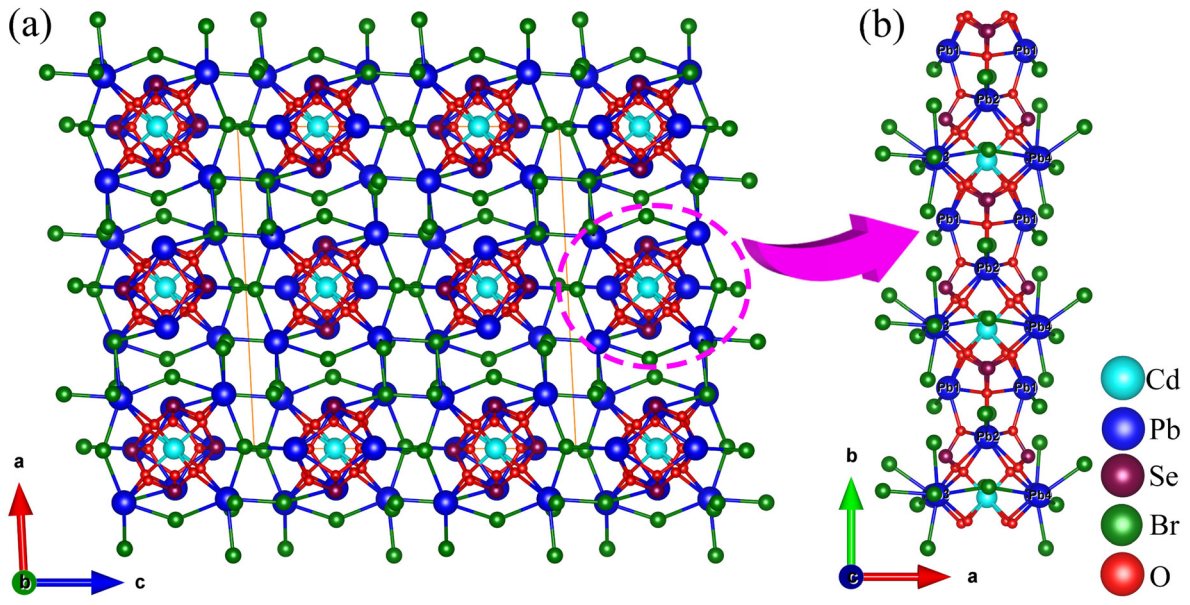


**Fig. 1** The 3D network structure (a) and the 1D chain component (b) of $CdPb_8(SeO_3)_4Br_{10}$.

 

form a 3D network with four-membered polyhedral ring (4-MR) tunnels (Fig. S2c†). The $[Cd(SeO_3)_4]^{6-}$ units and $Pb_4O_{12}Br_4$ tetramers are interconnected into one-dimensional (1D) chains along the *b*-axis (Fig. 1b and S2d†), which are located in the center of the 4-MR tunnels to support the framework.

$Pb_3(TeO_3)Br_4$ crystallizes in the NCS space group $Pna2_1$ (*No. 33*), isostructural with $Pb_3(TeO_3)Cl_4$ [49] and $Pb_3(SeO_3)Br_4$.[42] The asymmetric unit of the compound consists of a total of 11 atoms, which include three Pb, one Te, four Br, and three O atoms. All these atoms are located in general positions. The Te (1) atom adopts a $TeO_3$ trigonal pyramid coordination mode with Te–O bond lengths of 1.860–1.891 Å. The Pb atoms are coordinated with Br and O atoms with Pb–O and Pb–Br bond lengths in the range of 2.373–2.581 Å and 2.938–3.230 Å, respectively. Based on valence bond analysis, the oxidation states of lead and tellurium atoms are +2 and +4, respectively. The calculated values for Pb(1), Pb(2), Pb(3), and Te(1) are 1.797, 1.844, 1.640, and 3.984, respectively. Similarly, due to the neglect of longer secondary bonds involving $Pb^{2+}$ cations, the calculated oxidation states tend to be underestimated.[50] If longer Pb···Br and Pb···O distances were to be considered, the BVS of Pb(1)–Pb(3) can be raised to 1.943–1.967.

$Pb_3(TeO_3)Br_4$ exhibits a 3D framework composed of Pb–O–Br skeletons modified by $TeO_3$ groups (Fig. 2). The $Pb(1)O_2Br_3$, $Pb(2)O_1Br_5$, and $Pb(3)O_3Br_3$ polyhedra are connected *via* shared Br(1), Br(3), O(2) and O(3) atoms to form $Pb_3O_4Br_9$ trimers. These $Pb_3O_4Br_9$ trimers are interconnected through Pb–Br bonds to form a 1D chain with 4-MR tunnels along the *c*-axis. The $TeO_3$ groups are embedded in the center of the tunnels and connected to Pb atoms through bridging O atoms. The 1D chains are further interconnected *via* Pb–Br bonds to form the 3D framework structure (Fig. S3†).

To figure out the relationships between the macroscopic symmetries and the arrangements of building blocks, the local dipole moments of $CdPb_8(SeO_3)_4Br_{10}$ and $Pb_3(TeO_3)Br_4$ have been calculated. As shown in Table S3,† the polarity of the four selenite groups around the $CdO_6$ octahedron is almost cancelled out. Three quarters of the polarity of $Pb(3)_2Pb(4)_2$ 4-MR has been counteracted by the $CdO_6$ octahedron and $Pb_4O_{12}Br_4$ tetramer. Although the 1D chain component of $CdPb_8(SeO_3)_4Br_{10}$ is polar, the polarities of two neighbouring chains have been cancelled out completely. As for $Pb_3(TeO_3)Br_4$, the polarities of $TeO_3$ groups can be superimposed at *z*-components. Although the polarities of Te and Pb polyhedra are opposite, the 1D chain component is also polar. Furthermore, the polarities of the neighboring chains have been superimposed too, which leads to the NCS and polar space group of $Pb_3(TeO_3)Br_4$.

The thermal stability of $CdPb_8(SeO_3)_4Br_{10}$ and $Pb_3(TeO_3)Br_4$ was investigated through thermogravimetric analysis (TGA) in the temperature range of 25–1200 °C under an $N_2$ atmosphere. As shown in Fig. S4,† $CdPb_8(SeO_3)_4Br_{10}$ and $Pb_3(TeO_3)Br_4$ can remain stable up to 425 °C and 522 °C, respectively. After reaching these temperatures, both compounds began to experience weight loss. At 1200 °C, $CdPb_8(SeO_3)_4Br_{10}$ exhibited a total weight loss of 88.95%, corresponding to the loss of all $SeO_2$ and bromides of Cd and Pb, and partial loss of Pb oxides. $Pb_3(TeO_3)Br_4$ showed a weight loss of 80.13% (calculated value: 80.02%), equivalent to the loss of one molecule of $TeO_2$ and two molecules of $PbBr_2$.

The UV-vis-NIR diffuse-reflectance spectra reveal that $CdPb_8(SeO_3)_4Br_{10}$ and $Pb_3(TeO_3)Br_4$ are nearly transparent between 500 and 2000 nm. The UV absorption cutoff edges for these two compounds are 326 nm and 328 nm, respectively. Their band gaps were determined to be 3.32 eV and 3.31 eV, respectively (Fig. S5†), which are comparable to previously reported compounds, such as $Pb_2NbO_2(SeO_3)_2Br$ (3.17 eV),[41] $Ba(MoO_2F)_2(SeO_3)_2$ (3.23 eV),[34] $Lu_3F(SeO_3)_4$ (3.57 eV),[51] $Ag_2(TeO_2F_2)$ (3.22 eV)[52] and $Hg_3(Te_3O_8)(SO_4)$ (3.36 eV).[22]

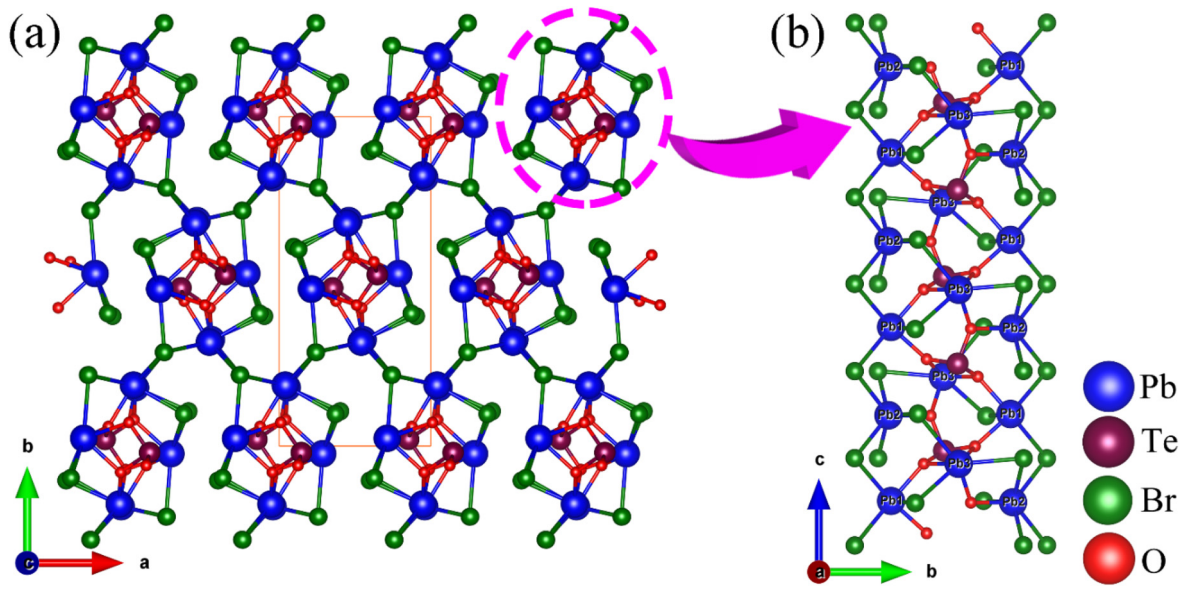


**Fig. 2** The 3D network structure (a) and the 1D chain component (b) of $Pb_3(TeO_3)Br_4$.

The infrared spectra (IR) demonstrate that $CdPb_8(SeO_3)_4Br_{10}$ and $Pb_3(TeO_3)Br_4$ exhibit good transparency in the range of 4000–775 $cm^{-1}$ (Fig. S6†). In particular, the absorption peaks at 400–455 $cm^{-1}$ can be attributed to the vibration of the Pb–O and Cd–O bonds. The prominent absorption peaks at 605–775 $cm^{-1}$ correspond to the bending and stretching vibrations of the Se–O and Te–O bonds, which are consistent with previous literature reports.[17,50] In summary, $CdPb_8(SeO_3)_4Br_{10}$ and $Pb_3(TeO_3)Br_4$ exhibit a wide transparency range of 0.33–12.96 μm and 0.33–12.95 μm, respectively. Considering the deviation of the IR cutoff edge for powder and crystal measurements due to multiphonon absorption, 50% eliminations were made.[53,54] So, the transparency range of $CdPb_8(SeO_3)_4Br_{10}$ and $Pb_3(TeO_3)Br_4$ should be 0.33–6.5 μm, covering an important atmospheric transparency window (3–5 μm) in the MIR region[28,55] (Fig. 3). This indicates that lead tellurite bromides could be potential NLO material systems in the MIR wavelength.

$Pb_3(TeO_3)Br_4$ possesses a large bandgap (3.31 eV), which tends to result in a high laser-induced damage threshold (LIDT). We measured the LIDT of $Pb_3(TeO_3)Br_4$ using the reported powder method. The LIDT of $Pb_3(TeO_3)Br_4$ is 21.5 MW $cm^{-2}$, which is significantly higher than that of $AgGaS_2$ (2.6 MW $cm^{-2}$).

Since the structure of $Pb_3(TeO_3)Br_4$ crystallizes in an NCS space group and contains two different nonlinear active units, it is necessary to detect its second-order nonlinear-optical response. A Q-switched Nd:YAG 1064 nm laser was chosen as the fundamental radiation, and the SHG signal was measured using the Kurtz–Perry method (ESI Experimental section†).[56] The SHG measurement indicates that $Pb_3(TeO_3)Br_4$ exhibits a frequency-doubling efficiency comparable to that of the commercial KDP (Fig. 4a). Compared with the SHG-inactive isomorphic compound $Pb_3(TeO_3)Cl_4$,[49] $Pb_3(TeO_3)Br_4$ shows a stronger SHG response, primarily attributed to the more polarizable property of the $Br^-$ anion compared with the $Cl^-$ anion.[42] In order to better understand the difference in the SHG effects between $Pb_3(TeO_3)Cl_4$ and $Pb_3(TeO_3)Br_4$, we compared the local dipole moments of the $TeO_3$ groups and $PbO_nX_m$ (X = Cl, Br) polyhedra, as well as the net dipole moments of these two compounds in their unit cells (Table S4†). The net dipole moment in the unit cell of $Pb_3(TeO_3)Cl_4$ is 8.68 D, while the net dipole moment in the unit cell of $Pb_3(TeO_3)Br_4$ is 10.062 D. The larger net dipole moment in $Pb_3(TeO_3)Br_4$ results in a larger SHG response compared to $Pb_3(TeO_3)Cl_4$. It is worth noting that $Pb_3(TeO_3)Br_4$ is the first example of tellurite bromide that has been detected to exhibit the SHG effect.

To investigate the electronic structures and optical properties of $CdPb_8(SeO_3)_4Br_{10}$ and $Pb_3(TeO_3)Br_4$, theoretical calculations based on the density functional theory (DFT) method were performed. The state energies of the lowest conduction band and the highest valence band are listed in Table S4.† As shown in Fig. S7,† $CdPb_8(SeO_3)_4Br_{10}$ is an indirect bandgap compound with a calculated bandgap of 2.955 eV, while $Pb_3(TeO_3)Br_4$ is a direct bandgap compound with a calculated bandgap of 3.134 eV. Due to the limitations of the DFT-GGA-PBE (GGA = generalized gradient approximation and PBE = Perdew–Burke–Ernzerhof) exchange–correlation functional, the calculated bandgaps are underestimated compared to the experimental values. Therefore, in the subsequent calculations, we employed a scissor operator with energy offsets of 0.365 eV and 0.176 eV, respectively.

The linear optical response characteristics of compounds $CdPb_8(SeO_3)_4Br_{10}$ and $Pb_3(TeO_3)Br_4$ were calculated based on the complex dielectric function $\varepsilon(\omega) = \varepsilon_1(\omega) + i\varepsilon_2(\omega)$. Both compounds belong to biaxial crystals, where the three principal permittivity coefficients are unequal, $\varepsilon_1 \neq \varepsilon_2 \neq \varepsilon_3$, and the refractive indices are also different, $n_1 \neq n_2 \neq n_3$. For $CdPb_8(SeO_3)_4Br_{10}$, the refractive index order is $n_{001} > n_{100} > n_{010}$. The calculated birefringence ($\Delta n$) values are 0.028@532 nm and 0.014@1064 nm (Fig. S8†), which are similar to those previously reported for compounds $La_2Hg_3(SeO_3)_4(SO_4)_2(H_2O)_2$ (0.013@532 nm and 0.008@1064 nm) and $Ag_2Cd(Se_2O_5)(Se_{0.3}S_{0.7}O_4)$ (0.026@532 nm and 0.022@1064 nm) by our group.[57] For $Pb_3(TeO_3)Br_4$, the refractive index order is $n_{100} > n_{010} > n_{001}$. The calculated birefringence ($\Delta n$) values are 0.095@532 nm and 0.066@1064 nm (Fig. 4b). It is worth noting that $Pb_3(TeO_3)Br_4$ exhibits a similar birefringence to those of pre-

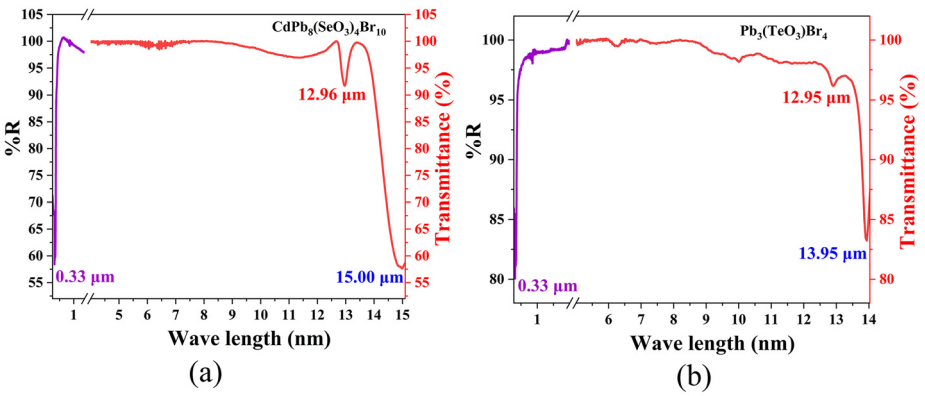


Fig. 3 UV-vis-NIR diffuse reflectance and IR transmittance spectra of $CdPb_8(SeO_3)_4Br_{10}$ (a) and $Pb_3(TeO_3)Br_4$ (b).

 

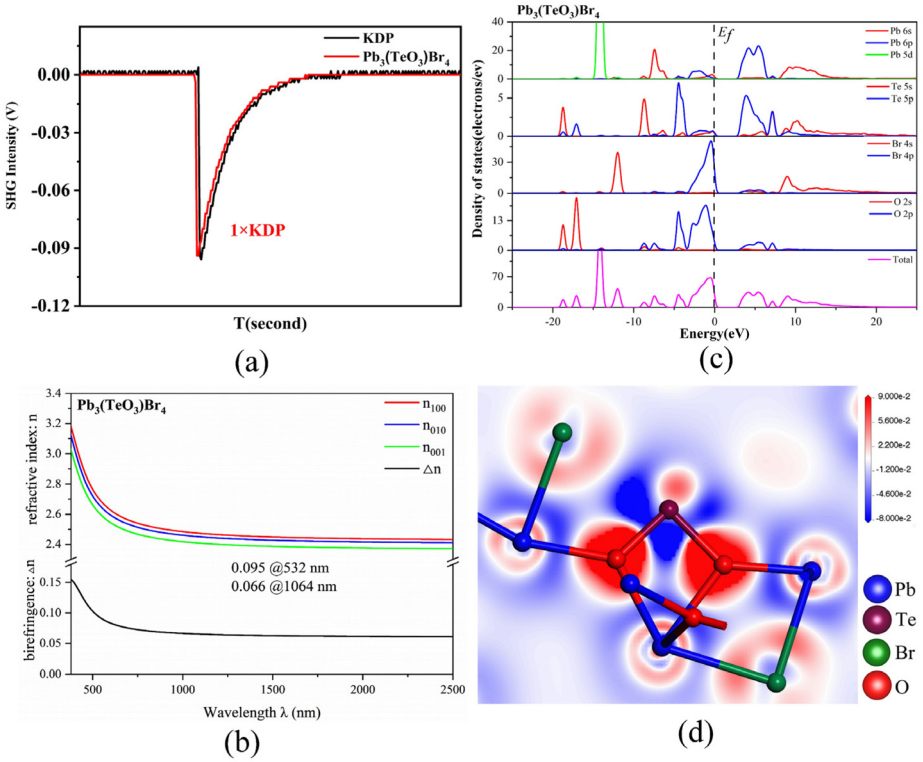


**Fig. 4** The oscilloscope traces of the SHG signals for the powder crystals (150–210 μm) of $Pb_3(TeO_3)Br_4$ and KDP under laser irradiation at 1064 nm (a). The total and partial density of states (b), the calculated refractive indices and birefringence (c) and the electron density difference (EDD) maps (d) of $Pb_3(TeO_3)Br_4$.

viously reported Te oxides, such as $Y_3(TeO_3)_2(SO_4)_2(OH)(H_2O)$ (0.092@532 nm),[15] $AgAl(Te_4O_{10})$ (0.104@532 nm),[19] $BaF_2TeF_2(OH)_2$ (~0.078@300–700 nm),[39] $Rb[Te_2O_4(OH)_5]$ (0.0545@1064 nm),[58] $Li_2ZrTeO_6$ (0.064@1064 nm)[59] and $AgTeO_2F$ (0.078@1064 nm).[52]

Partial density of states (PDOS) and total density of states (TDOS) calculations were performed for $CdPb_8(SeO_3)_4Br_{10}$ and $Pb_3(TeO_3)Br_4$. As shown in Fig. 4c, the lowest conduction bands of $Pb_3(TeO_3)Br_4$ mainly originate from the unoccupied Pb-6p orbitals and Te-5p orbitals, while the highest valence bands are mainly contributed by the Br-4p and O-2p non-bonding states. As for $CdPb_8(SeO_3)_4Br_{10}$, the lowest conduction bands are mainly from the unoccupied Pb-6p orbitals while the highest valence bands are mainly contributed by the Br-4p non-bonding states (Fig. S9†). Therefore, the band gap of $Pb_3(TeO_3)Br_4$ is mainly determined by the Pb and Te polyhedra, while the band gap of $CdPb_8(SeO_3)_4Br_{10}$ is mainly determined by the Pb–Br bonds.

It is worth noting that the states near the *Fermi* level have a significant impact on the linear and nonlinear properties of $Pb_3(TeO_3)Br_4$. The main influencing factors are Pb-6p, Te-5p, O-2p, and Br-4p orbitals in this compound. This indicates that the optical properties of $Pb_3(TeO_3)Br_4$ primarily originate from the synergistic interaction between the $TeO_3$ groups and the lead oxybromide polyhedra. To further support this inference, we have studied the electron density difference (EDD) map of $Pb_3(TeO_3)Br_4$. Fig. 4d shows that $Te^{4+}$ possesses stereo-chemically active lone pair electrons and there is charge transfer from Pb atoms to O/Br atoms.

## Conclusions

In summary, two new bromine-containing selenite/tellurite compounds, namely, $CdPb_8(SeO_3)_4Br_{10}$ and $Pb_3(TeO_3)Br_4$, were obtained by a mild hydrothermal method in the $Pb^{2+}$-$Se^{4+}O_3$/$Te^{4+}O_3$-$Br^-$ system. Interestingly, due to the difference in the arrangement of the polar building blocks, these two compounds exhibit two different lead oxybromide 3D structures. $CdPb_8(SeO_3)_4Br_{10}$ is crystallized in a CS space group of *C*2/*c* while $Pb_3(TeO_3)Br_4$ is crystallized in an NCS space group of $Pna2_1$. Importantly, $Pb_3(TeO_3)Br_4$ is the first reported tellurite bromide compound that exhibits SHG activity. It demonstrates an SHG intensity comparable to that of KDP, high thermal stability (522 °C), wide optical transparency window (0.33–6.5 μm) and appropriate birefringence (0.095@532 nm and 0.066@1064 nm). This work proved that lead tellurite bromides can be promising NLO material systems in the mid-IR wavelength.

## Conflicts of interest

There are no conflicts to declare.

## Acknowledgements

This work was supported by the National Natural Science Foundation of China (Grant No. 22031009, 22375201, 21921001 and 91963105) and the NSF of Fujian Province (Grant No. 2023J01216).

## References

1 L. Luo, L. Wang, J. Chen, J. Zhou, Z. Yang, S. Pan and J. Li, $A^{I}B_3^{II}C_3^{III}Q_8^{VI}$: A New Family for the Design of Infrared Nonlinear Optical Materials by Coupling Octahedra and Tetrahedra Units, *J. Am. Chem. Soc.*, 2022, **144**, 21916–21925.

2 P. F. Li, J. G. Mao and F. Kong, A survey of stereoactive oxysalts for linear and nonlinear optical applications, *Mater. Today Phys.*, 2023, **37**, 101197.

3 C. Yang, X. Liu, C. Teng, X. Cheng, F. Liang and Q. Wu, Hierarchical molecular design of high-performance infrared nonlinear $Ag_2HgI_4$ material by defect engineering strategy, *Mater. Today Phys.*, 2021, **19**, 100432.

4 M. Mutailipu, J. Han, Z. Li, F. Li, J. Li, F. Zhang, X. Long, Z. Yang and S. Pan, Achieving the full-wavelength phase-matching for efficient nonlinear optical frequency conversion in $C(NH_2)_3BF_4$, *Nat. Photonics*, 2023, **17**, 694–701.

5 P. F. Li, Y. P. Gong, C. L. Hu, B. Zhang, J. G. Mao and F. Kong, Four UV Transparent Linear and Nonlinear Optical Materials Explored from Pure Selenite Compounds, *Adv. Opt. Mater.*, 2023, 2301426, DOI: **10.1002/adom.202301426**.

6 H. Wang, Y. Chu, X. Pan, Z. Yang, S. Pan and J. Li, Double alkaline earth metals sulfide $SrMgGeS_4$ with high laser-induced damage threshold and strong second-harmonic generation, *Mater. Today Phys.*, 2023, **38**, 101243.

7 A. Tudi, C. W. Xie, S. L. Pan and Z. H. Yang, Design of novel deep-UV nonlinear optical materials with one-dimensional functional module $[BO_2]_\infty$ chain by fluorine-driven short phase-matching, *Mater. Today Phys.*, 2022, **28**, 100852.

8 H. Y. Wu, C. L. Hu, M. B. Xu, Q. Q. Chen, N. Ma, X. Y. Huang, K. Du and J. Chen, From $H_{12}C_4N_2CdI_4$ to $H_{11}C_4N_2CdI_3$: highly polarizable $CdNI_3$ tetrahedron induced a shape enhancement of second harmonic generation response and birefringence, *Chem. Sci.*, 2023, **14**, 9533–9542.

9 Y. Chu, H. Wang, T. Abutukadi, Z. Li, M. Mutailipu, X. Su, Z. Yang, J. Li and S. Pan, $Zn_2HgP_2S_8$: A Wide Bandgap Hg-Based Infrared Nonlinear Optical Material with Large Second-Harmonic Generation Response, *Small*, 2023, 2305074, DOI: **10.1002/smll.202305074**.

10 H. Chen, M. Y. Ran, S. H. Zhou, X. T. Wu, H. Lin and Q. L. Zhu, Simple yet extraordinary: super-polyhedra-built 3D chalcogenide framework of $Cs_5Ga_9S_{16}$ with excellent infrared nonlinear optical performance, *Chin. Chem. Lett.*, 2023, **34**, 107838.

11 J. H. Wu, B. Zhang, T. K. Jiang, F. Kong and J. G. Mao, From $Cs_8Sb_4Nb_5O_5F_{35}$ to $Cs_6Sb_4Mo_3O_5F_{26}$: the first noncentrosymmetric fluoroantimonite with $d^0$ transition metal, *Chin. J. Struct. Chem.*, 2023, **42**, 100016.

12 M. Y. Ran, S. H. Zhou, W. B. Wei, B. X. Li, X. T. Wu, H. Lin and Q. L. Zhu, Rational Design of a Rare-Earth Oxychalcogenide $Nd_3[Ga_3O_3S_3][Ge_2O_7]$ with Superior Infrared Nonlinear Optical Performance, *Small*, 2023, **19**, 2300248.

13 L. Wang, D. Chu, D. Yin, C. Xie, Z. Yang, J. Li and S. Pan, Theoretical investigations on ternary defective diamond-like infrared nonlinear optical materials in Be-Ga-Se system, *Mater. Today Phys.*, 2023, **38**, 101245.

14 P. F. Li, C. L. Hu, B. X. Li, F. Kong and J. G. Mao, $Y(HSeO_3)(SeO_3)(H_2O)\cdot(H_2O)$ and $Y_2(SeO_3)_2(SeO_4)(H_2O)_2\cdot(H_2O)_{0.75}$: Two yttrium selenites with a short UV cut-off edge explored from pure selenite compounds, *J. Alloys Compd.*, 2023, **959**, 170570.

15 P. F. Li, C. L. Hu, F. Kong, S. M. Ying and J. G. Mao, $Y_2(Te_4O_{10})(SO_4)$: a new sulfate tellurite with a unique $Te_4O_{10}$ polyanion and large birefringence, *Inorg. Chem. Front.*, 2021, **8**, 164–172.

16 S. Cho, S. Park, Y. Kuk and K. M. Ok, Elucidating the structure-nonlinear optical property relationship of $Te_2O_4(OH)_2$, *Mater. Today Phys.*, 2023, **34**, 101075.

17 Y. P. Gong, C. L. Hu, Y. X. Ma, J. G. Mao and F. Kong, $Pb_2Cd(SeO_3)_2X_2$ (X = Cl and Br): two halogenated selenites with phase matchable second harmonic generation, *Inorg. Chem. Front.*, 2019, **6**, 3133–3139.

18 X. L. Cao, C. L. Hu, F. Kong and J. G. Mao, Explorations of New SHG Materials in the Alkali-Metal-$Nb^{5+}$-Selenite System, *Inorg. Chem.*, 2015, **54**, 10978–10984.

19 P. F. Li, C. L. Hu, F. Kong and J. G. Mao, $AAl(Te_4O_{10})$ (A = Na, Ag) and $K_2Ga_2(HTe_6O_{16})(HTeO_3)$: Three Aluminum/Gallium Tellurites with Large Birefringence and Wide Band Gap, *Inorg. Chem.*, 2023, **62**, 8494–8499.

20 J. Li, W. D. Yao, J. N. Li, X. H. Li, W. Liu and S. P. Guo, Partial substitution induced structural transformation and enhanced nonlinear optical properties of $Na_2Ga_xIn_{6-x}Se_{10}$ (x = 3, 3.76), *Mater. Today Phys.*, 2023, **32**, 101007.

21 P. Wang, Y. Chu, A. Tudi, C. Xie, Z. Yang, S. Pan and J. Li, The Combination of Structure Prediction and Experiment for the Exploration of Alkali-Earth Metal-Contained Chalcopyrite-Like IR Nonlinear Optical Material, *Adv. Sci.*, 2022, **9**, 2106120.

22 P. F. Li, C. L. Hu, Y. P. Gong, F. Kong and J. G. Mao, $Hg_3(Te_3O_8)(SO_4)$: a new sulfate tellurite with a novel structure and large birefringence explored from $d^{10}$ metal compounds, *Chem. Commun.*, 2021, **57**, 7039–7042.

23 J. Zhou, Z. Fan, K. Zhang, Z. Yang, S. Pan and J. Li, $Rb_2CdSi_4S_{10}$: novel $[Si_4S_{10}]$ T2- supertetrahedra-contained infrared nonlinear optical material with large band gap, *Mater. Horiz.*, 2022, **10**, 619–624.

24 S. Han, A. Tudi, W. Zhang, X. Hou, Z. Yang and S. Pan, Recent Development of Sn(II), Sb(III)-based Birefringent Material: Crystal Chemistry and Investigation of Birefringence, *Angew. Chem., Int. Ed.*, 2023, **62**, e202302025.

 

25 Y. Long, X. Dong, L. Huang, H. Zeng, Z. Lin, L. Zhou and G. Zou, $BaSb(H_2PO_2)_3Cl_2$: An Excellent UV Nonlinear Optical Hypophosphite Exhibiting Strong Second-Harmonic Generation Response, *Mater. Today Phys.*, 2022, **28**, 100876.

26 C. Y. Meng, L. Geng, W. T. Chen, M. F. Wei, K. Dai, H. Y. Lu and W. D. Cheng, Syntheses, structures, and characterizations of a new second-order nonlinear optical material: $Pb_2(SeO_3)(NO_3)_2$, *J. Alloys Compd.*, 2015, **640**, 39–44.

27 K. C. Chen, C. S. Lin, G. Peng, Y. Chen, H. Z. Huang, E. Z. Chen, Y. X. Min, T. Yan, M. Luo and N. Ye, $LiNbTeO_5$: A High-Performance Multifunctional Crystal Material with a Very Large Second-Harmonic Generation Response and Piezoelectric Coefficient, *Chem. Mater.*, 2022, **34**, 399–404.

28 Q. Wang, X. H. Dong, L. Huang, K. M. Ok, Z. E. Lin and G. H. Zou, $Cd_2Nb_2Te_4O_{15}$ : A Novel Pseudo-Aurivillius-Type Tellurite with Unprecedented Nonlinear Optical Properties and Excellent Stability, *Small*, 2023, **19**, 2302797.

29 C. Li, Z. Gao, P. Zhao, X. Tian, H. Wang, Q. Wu, W. Lu, Y. Sun, D. Cui and X. Tao, Crystallographic Investigations into the Polar Polymorphism of $BaTeW_2O_9$: Phase Transformation, Controlled Crystallization, and Linear and Nonlinear Optical Properties, *Cryst. Growth Des.*, 2019, **19**, 1767–1777.

30 R. Robert, V. Balisetty, K. Mohanrao, M. Mannamala, S. Mangalassery, D. N. Rao and K. Vidyasagar, Syntheses, Crystal Structure, and Second Harmonic Generation Response of Noncentrosymmetric Layered Selenites and Tellurites of Antimony(v), $ASb_3Se_2O_{12}$ (A = K, Rb, Cs, Tl; X = Se, Te), *Inorg. Chem.*, 2023, **62**, 7890–7897.

31 J. Y. Chung, H. Jo, S. Yeon, H. R. Byun, T. S. You, J. I. Jang and K. M. Ok, $Bi_3(SeO_3)_3(Se_2O_5)F$: A Polar Bismuth Selenite Fluoride with Polyhedra of Highly Distortive Lone Pair Cations and Strong Second-Harmonic Generation Response, *Chem. Mater.*, 2020, **32**, 7318–7326.

32 X. Chen, Q. Jing and K. M. Ok, $Pb_{18}O_8Cl_{15}I_5$ : A Polar Lead Mixed Oxyhalide with Unprecedented Architecture and Excellent Infrared Nonlinear Optical Properties, *Angew. Chem., Int. Ed.*, 2020, **59**, 20323–20327.

33 P. F. Li, C. L. Hu, F. Kong and J. G. Mao, The First UV Nonlinear Optical Selenite Material: Fluorination Control in $CaYF(SeO_3)_2$ and $Y_3F(SeO_3)_4$, *Angew. Chem., Int. Ed.*, 2023, **62**, e202301420.

34 M. L. Liang, Y. X. Ma, C. L. Hu, F. Kong and J. G. Mao, $Ba(MoO_2F)_2(QO_3)_2$ (Q = Se, Te): Partial Fluorination of $MoO_6$ Octahedra Enabling Two Polar Solids with Strong and Phase Matchable SHG Response, *Chem. Mater.*, 2020, **32**, 9688–9695.

35 F. G. You, F. Liang, Q. Huang, Z. G. Hu, Y. C. Wu and Z. S. Lin, $Pb_2GaF_2(SeO_3)_2Cl$: Band Engineering Strategy by Aliovalent Substitution for Enlarging Bandgap while Keeping Strong Second Harmonic Generation Response, *J. Am. Chem. Soc.*, 2019, **141**, 748–752.

36 Y. J. Jia, X. Y. Zhang, Y. G. Chen, X. X. Jiang, J. N. Song, Z. S. Lin and X. M. Zhang, $PbBi(SeO_3)_2F$ and $Pb_2Bi(SeO_3)_2Cl_3$: Coexistence of Three Kinds of Stereochemically Active Lone-Pair Cations Exhibiting Excellent Nonlinear Optical Properties, *Inorg. Chem.*, 2022, **61**, 15368–15376.

37 X. L. Cao, C. L. Hu, F. Kong and J. G. Mao, $Cs(TaO_2)_3(SeO_3)_2$ and $Cs(TiOF)_3(SeO_3)_2$: structural and second harmonic generation changes induced by the different $d^0$-TM coordination octahedra, *Inorg. Chem.*, 2015, **54**, 3875–3882.

38 C. Wu, X. X. Jiang, L. Lin, Z. S. Lin, Z. P. Huang, M. G. Humphrey and C. Zhang, $AGa_3F_6(SeO_3)_2$ (A = Rb, Cs): A New Type of Phase-Matchable Hexagonal Tungsten Oxide Material with Strong Second-Harmonic Generation Responses, *Chem. Mater.*, 2020, **32**, 6906–6915.

39 J. J. Zhou, H. P. Wu, H. W. Yu, S. T. Jiang, Z. G. Hu, J. Y. Wang, Y. C. Wu and P. S. Halasyamani, $BaF_2TeF_2(OH)_2$: A UV Nonlinear Optical Fluorotellurite Material Designed by Band-Gap Engineering, *J. Am. Chem. Soc.*, 2020, **142**, 4616–4620.

40 Y. L. Hu, C. Wu, X. X. Jiang, Z. J. Wang, Z. P. Huang, Z. S. Lin, X. F. Long, M. G. Humphrey and C. Zhang, Giant Second-Harmonic Generation Response and Large Band Gap in the Partially Fluorinated Mid-Infrared Oxide $RbTeMo_2O_8F$, *J. Am. Chem. Soc.*, 2021, **143**, 12455–12459.

41 H. Zhao, P. Gong, X. Zhang, Z. Lin, Z. Hu and Y. Wu, Selenite bromide nonlinear optical materials $Pb_2GaF_2(SeO_3)_2Br$ and $Pb_2NbO_2(SeO_3)_2Br$: synthesis and characterization, *Dalton Trans.*, 2020, **49**, 14046–14051.

42 X. X. Wang, X. X. Jiang, H. M. Liu, L. Yang, Z. S. Lin, Z. G. Hu, X. G. Meng, X. G. Chen and J. G. Qin, $Pb_3(SeO_3)Br_4$: a new nonlinear optical material with enhanced SHG response designed via an ion-substitution strategy, *Dalton Trans.*, 2018, **47**, 1911–1917.

43 C. Shen, D. Sun, Y. Dang, K. Wu, T. Xu, R. Hou, H. Chen, J. Wang and D. Wang, $(C_4H_{10}NO)PbX_3$ (X = Cl, Br): Design of Two Lead Halide Perovskite Crystals with Moderate Nonlinear Optical Properties, *Inorg. Chem.*, 2022, **61**, 16936–16943.

44 T. Wang, Y. G. Chen, Y. Guo, F. Wang, Q. Song, Y. J. Jia and X. M. Zhang, $BaLiTe_2O_5X$ (X = Cl, Br): mixed alkali/alkaline-earth metal tellurite halides with $[Te_2O_5]_\infty$ chains, *Dalton Trans.*, 2020, **49**, 4914–4919.

45 X. H. Li, Z. H. Shi, M. Yang, W. Liu and S. P. Guo, $Sn_7Br_{10}S_2$ : The First Ternary Halogen-Rich Chalcohalide Exhibiting a Chiral Structure and Pronounced Nonlinear Optical Properties, *Angew. Chem., Int. Ed.*, 2022, **61**, e202115871.

46 D. Wang, Y. Zhang, Q. Shi, Q. Liu, D. Yang, B. Zhang and Y. Wang, Tellurate polymorphs with high-performance nonlinear optical switch property and wide mid-IR transparency, *Inorg. Chem. Front.*, 2022, **9**, 1708–1713.

47 S. M. Pei, B. W. Liu, W. F. Chen, X. M. Jiang and G. C. Guo, Breaking the Bottleneck of Simultaneously Wide Band Gap and Large Nonlinear Optical Coefficient by "Pore Reconstruction" Strategy in Salt-inclusion Chalcogenide, *Mater. Horiz.*, 2023, **10**, 2921–2926.

48 P. F. Li, F. Kong and J. G. Mao, $M_2^{II}M_3^{III}F_3(Te_6F_2O_{16})$ ($M^{II}$ = Pb, Ba; $M^{III}$ = Al, Ga): New mixed anionic tellurites with isolated $Te_6$ coplanar rings, *J. Solid State Chem.*, 2020, **286**, 121288.

49 S. Y. Zhang, C. L. Hu, P. X. Li, H. L. Jiang and J. G. Mao, Syntheses, crystal structures and properties of new lead(II) or bismuth(III) selenites and tellurite, *Dalton Trans.*, 2012, **41**, 9532–9542.

50 C. Bai, Y. Chu, J. Zhou, L. Wang, L. Luo, S. Pan and J. Li, Two new tellurite halides with cationic layers: syntheses, structures, and characterizations of $CdPb_2Te_3O_8Cl_2$ and $Cd_{13}Pb_8Te_{14}O_{42}Cl_{14}$, *Inorg. Chem. Front.*, 2022, **9**, 1023–1030.

51 C. Wu, L. H. Li, L. Lin, Z. P. Huang, M. G. Humphrey and C. Zhang, Enhancement of Second-Order Optical Nonlinearity in a Lutetium Selenite by Monodentate Anion Partial Substitution, *Chem. Mater.*, 2020, **32**, 3043–3053.

52 B. Zhang, J. H. Wu, C. L. Hu, Y. F. Li, F. Kong and J. G. Mao, From $AgTeO_2F$ and $Ag_2(TeO_2F_2)$ to $Ag_3F_3(TeF_6)(TeO_2)_{12}$: the first silver tellurite oxyfluorides with linear and nonlinear optical properties, *Inorg. Chem. Front.*, 2023, **10**, 1328–1337.

53 Z. Yang, C. Hu, M. Mutailipu, Y. Sun, K. Wu, M. Zhang and S. Pan, Oxyhalides: prospecting ore for optical functional materials with large laser damage thresholds, *J. Mater. Chem. C*, 2018, **6**, 2435–2442.

54 G. M. Li, Q. Liu, K. Wu, Z. H. Yang and S. L. Pan, $Na_2CdGe_2Q_6$(Q = S, Se): two metal-mixed chalcogenides with phase-matching abilities and large second-harmonic generation responses, *Dalton Trans.*, 2017, **46**, 2778–2784.

55 M. Y. Ran, A. Y. Wang, W. B. Wei, X. T. Wu, H. Lin and Q. L. Zhu, Recent progress in the design of IR nonlinear optical materials by partial chemical substitution: Structural evolution and performance optimization, *Coord. Chem. Rev.*, 2023, **481**, 215059.

56 S. K. Kurtz and T. T. Perry, A Powder Technique for the Evaluation of Nonlinear Optical Materials., *J. Appl. Phys.*, 1968, **39**, 3798–3813.

57 P. F. Li, C. L. Hu, F. Kong and J. G. Mao, $Hg_2(SeO_3)(SO_4)$: the first sulfate selenite with large birefringence explored from $d^{10}$ transition metal compounds, *Mater. Chem. Front.*, 2022, **6**, 3567–3576.

58 D. Wang, P. Gong, X. Zhang, Z. Lin, Z. Hu and Y. Wu, Centrosymmetric $Rb[Te_2O_4(OH)_5]$ and noncentrosymmetric $K_2[Te_3O_8(OH)_4]$: metal tellurates with corner and edge-sharing $(Te_4O_{18})^{12-}$ anion groups, *Inorg. Chem. Front.*, 2022, **9**, 2628–2636.

59 W. Lu, Z. Gao, X. Liu, X. Tian, Q. Wu, C. Li, Y. Sun, Y. Liu and X. Tao, Rational Design of a $LiNbO_3$-like Nonlinear Optical Crystal, $Li_2ZrTeO_6$, with High Laser-Damage Threshold and Wide Mid-IR Transparency Window, *J. Am. Chem. Soc.*, 2018, **140**, 13089–13096.